

# Laser-induced forward transfer of silver nanoparticle ink: time-resolved imaging of the jetting dynamics and correlation with the printing quality

Christos Boutopoulos · Ioannis Kalpyris ·  
Efthymis Serpetzoglou · Ioanna Zergioti

Received: 2 April 2013 / Accepted: 9 August 2013 / Published online: 22 August 2013  
© Springer-Verlag Berlin Heidelberg 2013

**Abstract** In this work, we used time-resolved imaging to study the dynamics of the laser-induced forward transfer (LIFT) process of a silver nanoparticle (NP) ink (NP size: 30–50 nm). LIFT is a versatile direct write technique in which a variety of functional materials can be transferred from a donor substrate to a receiving substrate with high spatial resolution. Two different LIFT configurations were employed: (a) dynamic release layer (DRL)-assisted LIFT, in which direct expose of the silver NP ink to laser irradiation is prevented, and (b) DRL-free LIFT, in which the silver NP ink is exposed to laser irradiation. Jetting dynamic behavior, initiated by a cavitation bubble generation and expansion, was observed in both LIFT configurations. However, jetting dynamics were significantly milder in the case of DRL-assisted LIFT, resulting in a wide laser fluence processing window (100–230 mJ/cm<sup>2</sup>) for high uniformity and reproducibility printing of silver NP ink droplets. On the contrary, DRL-free LIFT resulted in smooth jetting dynamics only for a narrow laser fluence window (30–40 mJ/cm<sup>2</sup>). The explanation of the different dynamics is based on the different mechanisms that govern the conversion of the laser pulse energy to a dynamic cavitation bubble for each LIFT configuration, i.e., (a) heat diffusion, mediated by the DRL layer, in DRL-assisted LIFT and (b) microcavitation around the silver NPs due to

near field enhancement when no DRL is used. In addition, the mechanism of formation of undesirable satellite droplets around the main deposited droplets was studied by using a flexible polymeric receiving substrate. The importance of the smooth jetting behavior, achieved by DRL-assisted LIFT, was highlighted for high-resolution printing of silver NP ink as well as for ensuring enhanced LIFT processing stability.

**Keywords** Laser-induced forward transfer · Silver nanoparticles ink · Microjets · Organic electronics · Microfabrication

## 1 Introduction

In recent years, the demand for smaller, lighter, and more affordable electronic devices has driven manufacturers toward new designs that incorporate organic electronics in commercial products such as solar and lighting panels. The use of metallic nanoparticle (NP) inks provides an excellent non-lithographic alternative for the fabrication of conductive interconnects for organic electronic devices since (a) it is compatible with rapid prototyping digital printing technologies (i.e., ink-jet printing (Cummins and Desmulliez 2012), laser direct write (Arnold et al. 2007)) and (b) it requires a relative low temperature post-printing curing step to ensure sufficient NPs' sintering, providing therefore a suitable patterning method when temperature-sensitive materials are used.

Despite its simplicity and broad appeal, the leading ink-jet printing technology presents several limitations when dealing with complex solutions such as metallic NP inks. In particular, the rheological properties of the silver NP ink suspensions should be carefully selected to avoid clogging

C. Boutopoulos · I. Kalpyris · E. Serpetzoglou · I. Zergioti (✉)  
Physics Department, National Technical University of Athens,  
Iroon Polytehneiou 9, 15780 Zografou, Athens, Greece  
e-mail: zergioti@central.ntua.gr

### Present Address:

C. Boutopoulos  
Engineering Physics Department, Laser Processing and  
Plasmonics Laboratory, École Polytechnique de Montréal,  
CP6079, Succ. Centre-ville, Montréal, QC H3C 3A7, Canada

of the print head nozzles (Cummins and Desmulliez 2012). Agglomeration of the suspended NPs can also lead to print head damage (Cummins and Desmulliez 2012). On the other hand, laser-induced forward transfer (LIFT) of complex solutions is receiving growing interest due to its unique application in printing cells (Schiele et al. 2010), biopolymers for chemical (Tsouti et al. 2010), and biological sensors (Boutopoulos et al. 2011; Chatzipetrou et al. 2013; Palla-Papavlu et al. 2010) as well as silver NP inks for organic electronics (Kim et al. 2009; Rapp et al. 2011). Printing of complex three-dimensional patterns has also been demonstrated by employing LIFT of high viscosity silver NP pastes (Wang et al. 2010).

A lot of research effort has been directed toward the optimization of the LIFT process of liquid solutions in the last years, including both experimental (Duocastella et al. 2012) and modeling studies (Brown et al. 2012). In addition, time-resolved imaging of the printing process has been employed by several research groups since it provides an advanced tool to study fast LIFT dynamics (Brown et al. 2011; Duocastella et al. 2010; Duocastella et al. 2009; Unger et al. 2010; Yan et al. 2012). Most of these studies deal with model glycerol-based solutions and employ a dynamic release layer (DRL)-assisted LIFT configuration. Researchers conclude that under the optimum laser fluence, the ejection of the liquid takes place through the formation of a long and stable jet. It has also been shown that droplet's growth on the receiving substrate starts when the jet impinges on the receptor substrate (Duocastella et al. 2010; Unger et al. 2010). Following the jet impingement on the receptor substrate, the liquid starts accumulating gently on the impact position forming a sessile drop, which relaxes in its final shape in a microsecond time scale (Duocastella et al. 2010). Those studies on model glycerol-based solutions have provided valuable information for improving the performance of the technique. However, when LIFT is applied to complex solutions (i.e., silver NP inks), several aspects concerning the printing process require further investigation to optimize the capabilities of technique in terms of resolution and reproducibility. These include (a) the formation of undesirable satellite droplets around the main deposited droplet and (b) the existence of a narrow laser process window for uniform printing when DRL is not used (Duocastella et al. 2012; Rapp et al. 2011).

In this study, we focused on the LIFT dynamics of a commercially available silver NP ink, aiming to interconnect printing optimization. Time-resolved imaging was used to investigate the dynamics of both DRL-assisted and DRL-free LIFT of the silver NP ink. Jetting behavior was observed during the ejection of the ink for both LIFT configurations. In particular, smooth high-aspect-ratio silver NP ink jets were generated under optimum laser conditions. However, jetting dynamics and jets'

morphology were found to depend strongly on the LIFT configuration. The explanation for the different dynamics was based on different mechanisms that govern the conversion of the laser pulse energy to a dynamic cavitation bubble. The jetting dynamics of the silver NP ink was correlated with the deposition quality on polymer substrate [polyethylene naphthalate (PEN)], a commonly used substrate on organic electronics. Emphasis was given to the mechanism that causes the deposition of undesirable satellite droplets.

## 2 Experimental

### 2.1 LIFT setup

The experimental setup used in this study is depicted in Fig. 1. Laser printing of the silver NP ink was achieved by using a pulsed Nd:YAG (yttrium aluminum garnet) laser (266-nm wavelength, 10-ns pulse duration) and a mask projection optical setup composed of a beam expander, a variable circular mask, an attenuator, and a converging lens. The imaging system was adjusted to a demagnification factor of 5 (1/M), resulting in a 50- $\mu$ m spot size at the imaging plane.

### 2.2 Donor substrate preparation

Two different types of supports were used for the donor substrate preparation (Fig. 2). The first type consists of 1-mm-thick quartz plates (25 mm in diameter) purchased from UQG Optics. The second type of supports was prepared by using the same type of quartz plates coated with a 40-nm titanium laser-absorbing layer. A thin liquid film of silver NP ink (U5603, SunChemicals, 20 wt% silver content, solvent: mixture of ethylene glycol, glycerol, and ethanol, viscosity: 12 mPa s, NP size: 30–50 nm) was applied to both types of donor substrates by using spin coating (2900 rpm, 30 s). Spin coating ensured reproducibility and high uniformity of the film thickness ( $\sim 5.5$   $\mu$ m) across the donor target surface. No additional treatment was applied at the donors, which were used for a maximum period of 30 min after their preparation to avoid silver NP ink film drying (Boutopoulos et al. 2013a). The reflectivity of the titanium DRL/silver NP ink/quartz donors at 266 nm was experimentally defined to be around 25 %, while in the case of the silver NP/quartz donors, the reflectivity was negligible. The reflectivity of the donors is taken into account at the discussion part, where a comparison between the different jetting dynamics is presented. In particular, we compare results at a certain absorbed laser fluence (i.e.,  $(1-R) \times I_0$ ), where R and  $I_0$ , represent the reflectivity of the donors and the incident laser fluence, respectively.

**Fig. 1** Schematic illustration depicting the laser-induced forward transfer (LIFT) experimental setup as well as the pump-probe ultrafast imaging setup

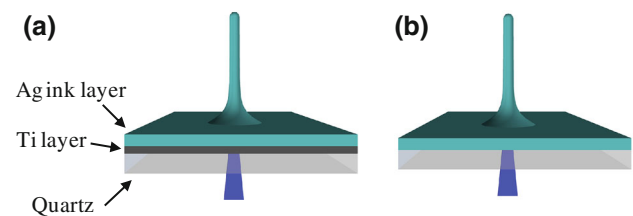
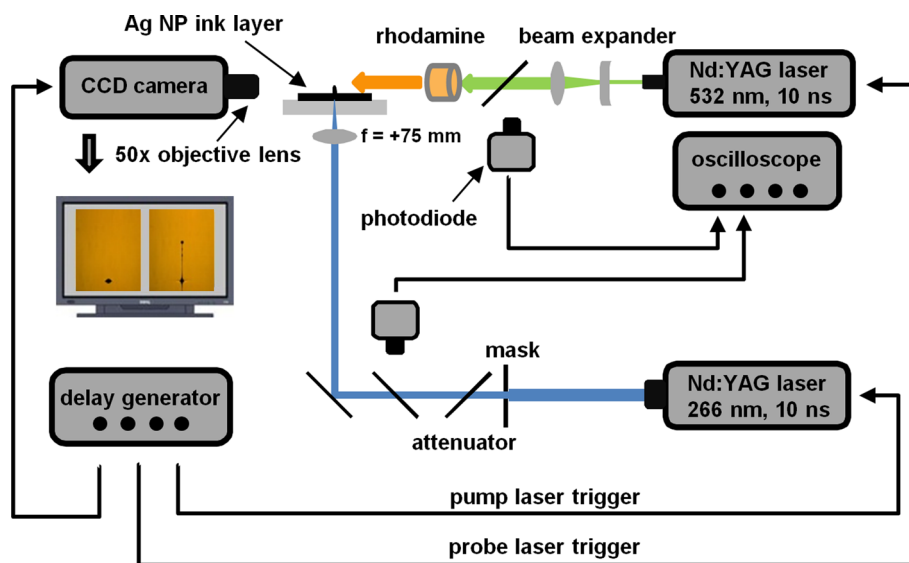


**Fig. 2** Schematic illustration representing the two donor configurations used in our study: **a** quartz support/titanium layer/silver NP ink layer, **b** quartz support/silver NP ink layer. Not to scale

### 2.3 Time-resolved imaging setup

In the first part of this work, the donor substrates were placed in “face up” LIFT configuration without receiving substrate for the side-view imaging of the printing process (Fig. 2). Pump–probe experiments were then applied for high-speed shadowgraphic imaging of the process using both types of donor substrates as described below. A second Nd:YAG laser (532-nm wavelength, 10-ns pulse duration) was used to pump a fluorescence dye (rhodamine solution) in transparent container placed on the camera axis. The technique allows for high-quality imaging due to the emission of incoherent light from the dye (Fardel et al. 2009). Capturing of shadowgraphic images was achieved by a CCD camera (Unibrain Fire-i 810) equipped with a 50X long working distance objective lens placed perpendicular to the laser printing axis. The trigger of the CCD camera as well as the pump and probe laser synchronization was initiated by a pulse delay generator (DG535, Stanford Research Systems), which allowed setting the delay between the printing and illuminating laser pulses. The exact delay between the two pulses was measured using two photodiodes connected to an oscilloscope.

In the second part of this work, time-resolved analysis of the silver ink droplets formation was performed by using the same configuration and PEN-receiving substrates. Copper spacers were used to fix the donor and receiving substrates at a separation distance ranging from 180 to 250 μm. The series of images were taken by moving the donor-receiving substrate assembly in the x or y direction so as an unused region was irradiated for each image frame.

Three to five images were taken for each delay time to ensure reproducibility. The analysis of the images was carried out by using the ImageJ software to extract the front distance of the ejected material as a function of the time. The morphological characterization of the deposited droplets was performed by optical microscopy.

## 3 Results and discussion

### 3.1 Jetting dynamics during LIFT of silver NP ink using titanium as dynamic release layer

Figure 3 depicts a series of shadowgraphic time-resolved images of silver NP ink ejection for various laser fluences using titanium as DRL on quartz donor substrates. It is a common observation for the entire laser fluence range that the ejection of the silver NP ink material is initiated by the formation of a conical liquid protrusion (first frame in Fig. 3a–e). Its dynamic growth and expansion is strongly depended on the laser fluence conditions as it is discussed below. The driving force for the formation of the initial liquid protrusion comes from the generation of high-pressure cavitation bubble at the titanium layer/silver NP ink interface following the laser irradiation. In particular, the absorption of the incident laser pulse by the 40-nm-thick

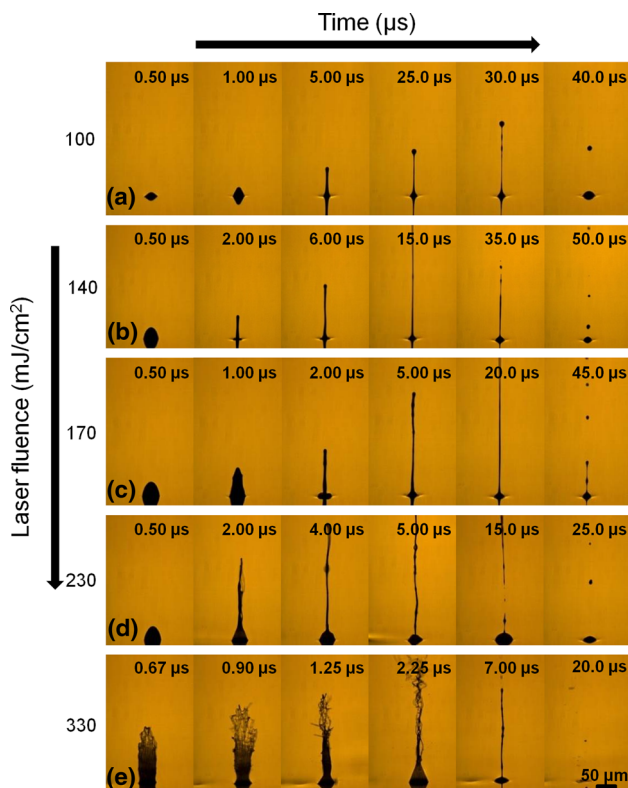


**Fig. 3** Series of time-resolved images of the silver NP ink ejection by using Ti/quartz donor substrates and various laser fluences: **a** 100 mJ/cm<sup>2</sup>, **b** 140 mJ/cm<sup>2</sup>, **c** 170 mJ/cm<sup>2</sup>, **d** 230 mJ/cm<sup>2</sup> and **e** 330 mJ/cm<sup>2</sup>. Each series of pictures was taken by varying the time delay between the pump and probe laser pulses

titanium layer results in a temperature rise, which causes localized evaporation of the silver NP ink's solvents. In accordance with the absorption coefficient ( $\alpha \sim 5.96 \times 10^5 \text{ cm}^{-1}$ ) of the Ti layer at 266 nm (Lynch et al. 1975), the incident laser radiation will not exceed a penetration depth of about 17 nm ( $1/\alpha$ ). Therefore, for the first series of our experiments, we consider negligible direct exposure of the silver NP ink to the laser pulse, since the penetration depth is much shorter than the titanium DRL thickness (40 nm).

In our experiments, the initial conversion of the laser pulse energy to heat and vapor pressure is followed by a complex hydrodynamic process that governs the silver NP ink ejection. The expanding cavitation bubble, generated in between the donor substrate and the silver NP ink-free surface, propels forward the overlying silver NP ink layer. When the interior driving force overcomes the viscous and surface forces, a conical protrusion starts growing at the free surface of the thin liquid film as it can be seen in Fig. 3. This process, depending on the laser fluence, lasts a time period that is ranged from about 0.5 to 2  $\mu\text{s}$ . Analogous, but much slower processes (millisecond time scale) have been thoroughly studied in the literature, when millimeter-sized cavitation bubbles were generated near a free

liquid surface using either electrical discharge (Robinson et al. 2001) or focused laser beams (Blake and Gibson 1981).

At 100 mJ/cm<sup>2</sup> (Fig. 3a), the kinetic energy of the initial conical protrusion is sufficient to overcome the pull-off forces. This critical condition leads to the formation of a thin and directional silver NP ink jet that gently detaches the liquid film. Further increment in the laser fluence beyond the jetting threshold results in the formation of higher velocity detaching jets (Fig. 3b, c). In this laser fluence range (140–170 mJ/cm<sup>2</sup>), the jets remain directional while presenting a more elongated shape. The typical diameter of the jets at their narrower point is about 4  $\mu\text{m}$ , and their longitudinal dimension exceeds the frame height ( $\sim 400 \mu\text{m}$ ). Depending on the laser fluence, the smooth and continuous shape of the jets brakes over a certain time period. This can be clearly seen in some late frames of Fig. 3, where the gently growing jets present several small perturbations and finally brake up in multiple satellite droplets and/or secondary thin liquid threads detached from the initial jet. This is the result of the so-called Plateau–Rayleigh instability that is common for liquid streams (Eggers 1997), where the surface tension-dominated phenomena induce a geometry that ensures a minimal energy state.

Further increment of the laser fluence results in the generation of less uniform silver NP ink jets as it can be seen in Fig. 3d (230 mJ/cm<sup>2</sup>). However, the jetting behavior remains directional with a faster evolution dynamics (i.e., the jet is completely detached within 25  $\mu\text{s}$ ). The materials' ejection becomes turbulent at a laser fluence of 330 mJ/cm<sup>2</sup> (Fig. 3e). In particular, 0.9  $\mu\text{s}$  after the pump laser pulse, the ejected silver NP ink material reserves a plume-like shape. Beyond the 1.25  $\mu\text{s}$ , a conical liquid formation appears due to the convergence of the outer part of the plume-like formation. A turbulent jet flow is then initiated, which finally decays in several satellite droplets in a time period of about 20  $\mu\text{s}$ . Notice that the faster jetting dynamics at high laser fluence (230–300 mJ/cm<sup>2</sup>) resulted in jet breaking at significantly shorter times compared to relative low laser fluence experiments (100–170 mJ/cm<sup>2</sup>).

The corresponding jet velocity for the various laser fluences can be found in Table 1. Each velocity value was calculated by a linear fit of the jet front distance dependence on the time. The calculated velocities vary from 9 to 77 m/s for laser fluences ranging from 100 mJ/cm<sup>2</sup> (jetting threshold) to 230 mJ/cm<sup>2</sup> (turbulence threshold), respectively. At the high turbulent jetting regime (330 mJ/cm<sup>2</sup>), the velocity of the jet reaches the 96 m/s. However, this velocity range is well below the supersonic ejection regime and therefore justifies the absence of shock-wave formation in Fig. 3.



**Table 1** The calculated jet velocities for the two donor configurations

Donor substrate : Ti layer/quartz		Donor substrate : Quartz	
Laser fluence (mJ/cm <sup>2</sup> )	Velocity <sup>a</sup> (m/s)	Laser fluence (mJ/cm <sup>2</sup> )	Velocity <sup>a</sup> (m/s)
100	9 ± 2 <sup>b</sup>	20	27 ± 2 <sup>b</sup>
140	42 ± 3	30	80 ± 3
170	45 ± 5	40	105 ± 8
230	77 ± 5	50	171 ± 14
330	96 ± 13	70	237 ± 14

<sup>a</sup> The velocity was calculated by a liner fit of the jet front distance dependence on time

<sup>b</sup> The velocity error corresponds to the standard error of the linear fit slope

Similar dynamic behaviour has been reported by Duocastella et al. (2009) where LIFT of model glycerol-based solution was studied using similar experimental conditions to our study (i.e., ns UV pulses, 50-nm-thick titanium DRL layer). However, in our study, the emergence of the different ejection regimes is shifted to significantly lower laser fluences. This is attributed to the reduced thickness of the silver NP ink film (~5.5 μm) compared with the thickness of the glycerol-based ink film (~20 μm) used in Duocastella’s study. On the contrary, our recent time-resolved imaging study on DRL-assisted LIFT of silver NP inks did not disclose jetting dynamics (Boutopoulos et al. 2013a). Indeed, the selection of relative large laser spot size (220 μm) compared with the silver NP ink layer thickness (~5.5 μm) resulted in materials’ ejection that clearly reproduced the size and the shape of the laser spot.

### 3.2 Jetting dynamics during LIFT of silver NP ink without using dynamic release layer

In the second series of experiments, time-resolved shadowgraphic imaging was employed to investigate the jetting dynamics of the LIFT process without using DRL. Figure 4 depicts a series of images of silver NP ink ejection for various laser fluences using quartz donor substrates. The mechanism of the silver NP ink ejection is considered similar to the one described in the previous section (i.e., cavitation bubble generation, initial ink protrusion formation, and expansion); however, significantly faster dynamic behavior is observed.

In particular, smooth jetting behavior is observed only for a laser fluence of 20 mJ/cm<sup>2</sup> that corresponds to the ejection threshold (Fig. 4a). A slight increase in the laser fluence over the ejection threshold results in turbulent jetting behavior as it can be seen in Fig. 4b. For higher laser fluences, over the 30 mJ/cm<sup>2</sup>, the high internal pressure of

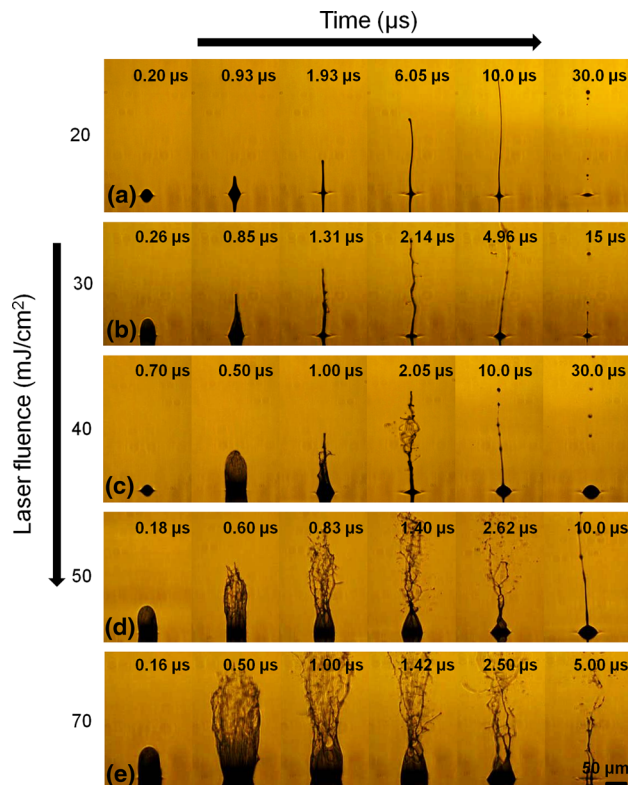


**Fig. 4** Series of time-resolved images of the silver NP ink ejection by using quartz donor substrates and various laser fluences: **a** 20 mJ/cm<sup>2</sup>, **b** 30 mJ/cm<sup>2</sup>, **c** 40 mJ/cm<sup>2</sup>, **d** 50 mJ/cm<sup>2</sup>, and **e** 70 mJ/cm<sup>2</sup>. Each series of pictures was taken by varying the time delay between the pump and probe laser pulses

the initial plume-like protrusion (second frame in Fig. 4c–e) overcomes the coherent forces of the liquid resulting in a violent expansion within a 0.5-μs time period. Past the rapid pressure release, the coherent forces of the liquid cause a convergence of outer part of the plume. This process takes place within a time period of about 1 μs (third frame in Fig. 4c–e). The resulted turbulent conical ejection of the silver NP ink material (late frames in Fig. 4c–e) is similar to the one observed in the previous section for significantly higher laser fluence (Fig. 3e).

The corresponding jet velocity for the various laser fluences can be found in Table 1. As in the case of the DRL-assisted LIFT experiments, the ejection velocities were derived from a linear fit of jet front distance dependence on time. The ejection velocities vary from 27 to 237 m/s for a laser fluence range from 20 mJ/cm<sup>2</sup> (ejection threshold) to 70 mJ/cm<sup>2</sup>, respectively. A comparison between the two velocity columns of Table 1 reveals significantly faster ejection in the case of silver NP ink LIFT without using DRL. In particular, a careful look at a certain laser fluence range (i.e., 70–75 mJ/cm<sup>2</sup>) after deducting the reflected part of the beam (i.e., LIFT with DRL: (1–R<sub>Ti</sub>) × 100 mJ/cm<sup>2</sup> ~ 75 mJ/cm<sup>2</sup>, LIFT without DRL: (1–

$R_{\text{ink}} \times 70 \text{ mJ/cm}^2 \sim 70 \text{ mJ/cm}^2$ ) proves about 20 times faster jets in the case of LIFT without using DRL. However, the maximum ejection velocity is again well below the supersonic threshold, and therefore, no shock-wave propagation is observed.

Further information regarding the considerable faster dynamics for DRL-free LIFT can be derived by comparing the different jetting regimes in Figs. 3 and 4. When no DRL is used (Fig. 4a), the ejection threshold ( $20 \text{ mJ/cm}^2$ ) is almost 4 times lower compared to the one observed in the case of titanium DRL-assisted LIFT (Fig. 3a) after deducting the reflected part of the beam  $[(1-R_{\text{Ti}}) \times 100 \text{ mJ/cm}^2 \sim 75 \text{ mJ/cm}^2]$ . In addition, when no DRL is used, the laser processing window for smooth jetting behavior is defined less than 0.5 times the laser fluence threshold (Fig. 4a, b), while in the case of DRL-assisted LIFT is extended to 1.3 times the laser fluence threshold (Fig. 3a–d).

The observed dependence of the jetting dynamics on the laser fluence provides an explanation for the existence of a narrow laser processing window for LIFT printing of uniform Ag NP ink patterns when no DRL is used (Duocastella et al. 2012; Rapp et al. 2011). In those studies, the morphological characterization of the LIFT printed Ag ink droplets revealed that a slight increase in the laser fluence over the optimum conditions resulted in droplets' non-uniformity and satellite droplets formation. This is attributed to the observed fast and turbulent ejection dynamics (Fig. 4), and it will be more thoroughly discussed in the next section. Both phenomena are undesirable when considering a potential commercialization of the process. Indeed, slight laser fluence variation would be reflected to significant process instability. A relative observation has been reported by Lewis et al. (2006), where the authors mentioned an "inconsistent" ejection of the ink jet beyond the threshold fluence without providing any further analysis.

The presence of significantly faster dynamics when LIFT of silver NP ink was performed without using DRL is mainly attributed to the direct exposure of a significant part of the silver NP ink layer to laser irradiation. When LIFT was performed without using DRL, the laser irradiation penetrated within the first  $\sim 1.6 \mu\text{m}$  [experimentally defined in (Boutopoulos et al. 2013a)] of the silver NP ink layer ( $\sim 5.5 \mu\text{m}$  total thickness). The laser-induced heating of the off-resonance 30–50 silver NPs, as well as the strong near-field enhancement around the vicinity of the NPs [nanolens effect (Nedyalkov et al. 2010)], contributed to the generation of several nanobubbles within the laser penetration depth. The dynamics of the nanobubble generation around metallic NPs has been reported to be extremely fast (nanosecond time scale) (Brujan 2011; Lapotko 2009). It has also been shown that the maximum

diameter of the nanobubbles scales with the square root of the laser fluence (Brujan 2011). The synergetic action of the bubbles, which were generated immediately after the laser irradiation, results in the formation of a larger cavitation bubble that expands as observed in Fig. 4. This mechanism of the cavitation bubble formation is considered as the dominant factor for the observed accelerated dynamics compared to DRL-assisted LIFT, where the cavitation bubble formation is mainly induced by the temperature rise on the titanium layer/silver NP ink interface.

### 3.3 Deposition process and satellite droplets' formation

In the third series of experiments, we selected the DRL-assisted LIFT to study the dynamics the droplet deposition in order to understand the mechanism of the satellite droplets formation. Our selection to focus in DRL-assisted LIFT is in accordance with previous sections finding, where the use of the titanium DRL has been proved ideal for achieving controllable jetting dynamics. PEN-receiving substrates were placed at distances between 180 and  $250 \mu\text{m}$  opposite to the donor substrate by using appropriate spacers.

Figure 5a, c and e shows a series of time-resolved images that correspond to various jetting regimes described in Sect. 3.1. Optical microscopy images of corresponding droplets, deposited under identical printing conditions, are shown in Fig. 5b, d and f, respectively. At a laser fluence of  $100 \text{ mJ/cm}^2$  (Fig. 5a, jetting threshold), optimum printing conditions were observed. The low-velocity (9 m/s) jet impingement on the receiving substrate is followed by a gentle liquid accumulation at the initial point of impact. This results in the formation of a uniform silver NP ink drop (Fig. 5b) on the PEN substrate. The droplets' feeding with ink last about  $100 \mu\text{s}$  and then jets' breakup take place. Similar, but quite faster dynamics were observed when the laser fluence was increased to  $200 \text{ mJ/cm}^2$  (Fig. 5c). The impact velocity of the jet is about 50 m/s, and its shape and evolution remain smooth. Breakup takes place within less than  $20 \mu\text{s}$ , while the deposited droplets preserve a uniform shape (Fig. 5d).

A careful observation on Fig. 5b and d reveals that despite the smoothness of the droplets formation process, there is a possibility for satellites droplet formation around the main deposited droplet. These satellite droplets are shown as small debris in Figs. 5b and 4c. Their formation is attributed to the generation of small droplets during jets breakup as it can be seen in Figs. 5a and 4c. Those droplets are mainly incorporated into the main droplet's body; however, they may be deposited as satellite droplets due to a divergence of their travel. This effect can be eliminated by improving the vibration isolation of the experimental

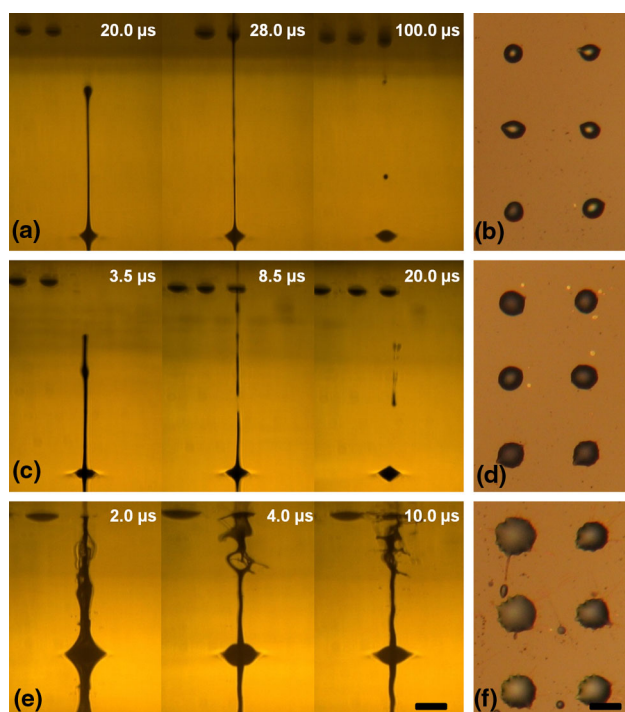


**Fig. 5** Titanium DRL-assisted LIFT of silver NP ink. Time-resolved imaging of LIFT process for various laser fluences showing jets impingement on PEN-receiving substrates. Optical microscopy images of the corresponding deposited droplets are also presented: **a, b** 100 mJ/cm<sup>2</sup> (ejection threshold), **c, d** 200 mJ/cm<sup>2</sup> (smooth jetting regime), **e, f** 230 mJ/cm<sup>2</sup> (turbulent jetting regime). The scale bar corresponds to 50 microns

setup as well as by reducing the distance between the donor and the receiving substrate.

The droplet formation process is dramatically affected when the laser fluence is increased to generate a higher velocity jet (77 m/s). Figure 5e shows the impingement of a high-velocity turbulent jet, generated by a laser fluence of 230 mJ/cm<sup>2</sup>, on the PEN-receiving substrate. Following the initial jet impact to the receiving substrate, recoil of the ink is observed. The recoiled ink strongly interfering with the evolution of the initial ejected jet, resulting in a turbulent morphology that is mainly detected close (around 100 μm) to the receiving substrates' surface (second and third frame in Fig. 5e). Figure 5f shows the optical microscopy images of the corresponding deposited droplets, where several satellite droplets can be found. Their formation is a result of the violent jets breakup close to PEN surface. In particular, main jets breakup generated several smaller sub-jets randomly directed in the space around the main drop. Subsequently, their impingement on the PEN surface and/or their breakup caused the satellite droplets deposition.

The observed jet recoil based mechanism of satellites droplets formation is rather depended on the properties of the ink (i.e., surface tension, viscoelasticity, impinge

velocity) than jet morphology itself. Another factor that significantly affects the jet recoil process is the wetting properties of the receiving substrate. Indeed, jet recoil may be caused when smooth, low-velocity jets impinge hydrophobic surfaces as we have recently shown in a relative study (Boutopoulos et al. 2013b). In the recent LIFT bibliography on glycerol-based model solutions printing, the satellite droplets generation has been mainly linked to the so-called plume ejection regime (i.e., high turbulent non-jetting liquid ejection) (Duocastella et al. 2009) and/or to the jet breakup due to Plateau–Rayleigh instability (Duocastella et al. 2010), depending on the laser fluence. Unger et al. (2010) have mentioned the creation of satellite droplets due to main droplets' splashing when LIFT of a hydrogel was performed at high-velocity jetting conditions. Slight splashing behavior can also be observed in our experiments (i.e., ink material laterally detached from the main drops' body, Fig. 5e and other not shown), but it is not considered as the main mechanism for satellite droplets deposition for the studied laser fluence range. Indeed, the main mechanism is considered the recoil of the ink due to the relative high-velocity jet impingement on PEN surface. However, the low-velocity ejection achieved by the DRL-assisted LIFT prevents the generation of the satellite droplets due to jet recoil for a sufficient laser fluence range (100–200 mJ/cm<sup>2</sup>).

#### 4 Conclusion

Time-resolved imaging of LIFT of a silver NP (NP size: 30–50 nm) ink revealed jetting ejection dynamics for two different donor configurations; (a) a ~ 5.5-μm-thick NP ink layer spread on a titanium covered (40-nm thick) quartz plate (i.e., DRL-assisted LIFT) (b) a ~ 5.5-μm-thick NP ink layer spread on quartz plate (i.e., DRL-free or conventional LIFT). In both donor configurations, jetting behavior was initiated by an expanding cavitation bubble generated in between the donor surface and the ink-free surface. When titanium DRL was used, the conversion of the laser pulse energy to impulse pressure was governed by the heat diffusion to the ink layer, mediated by the titanium layer. On the contrary, LIFT without using DRL involves direct exposure of the silver NP ink to laser irradiation, resulting in NPs heating and near field enhancement around the NPs vicinity. Both phenomena contribute to the instant generation of several nanobubbles within the ink medium, providing therefore the impulse force for materials' ejection. The different mechanisms involved in the generation of the cavitation bubble caused significantly variation to the observed jetting dynamics. In particular, titanium DRL-assisted LIFT resulted in smooth and low-velocity (9–77 m/s) jetting behavior, for a wide laser process window

(100 mJ/cm<sup>2</sup>–230 mJ/cm<sup>2</sup>), indicating therefore a great potential for a high-quality direct-printing process. On the other hand, when LIFT was performed without using DRL, a narrow laser process window (20–30 mJ/cm<sup>2</sup>) was observed for reliable jetting behavior (27–80 m/s).

The last part of our work discloses importance of the smooth, low-velocity jetting dynamics for the deposition of debris-free silver NP ink droplets on PEN substrates. On the contrary, high-velocity jetting dynamics resulted in the generation of undesirable satellite drops around the main deposited ink drop. The main mechanism for the satellite depositions was found to be the interference of the ink, recoiled from a receiving substrate, with the initial jet. The laser fluence threshold for this behavior was 230 mJ/cm<sup>2</sup>, and the corresponding jet velocity is 77 m/s for DRL-assisted LIFT. Low-velocity impingement of the jet to the receiving surface is therefore proposed to eliminate satellite drops deposition. The use of the titanium DRL significantly expands the laser process window that optimum laser deposition conditions can meet.

Therefore, its use for conductive interconnect printing optimizes the capabilities of the LIFT technique in terms of resolution and process stability. Many applications can be benefit by the technique including the integration of conductive electrodes during the fabrication of microfluidic devices, where LIFT printing offers a great alternative to conventional sputtering and ink-jet printing technologies. More advanced applications can be triggered in transparent microfluidic devices, where laser pulses may be used to control microflows by generating cavitation bubbles and microjets in the microfluidic channels.

**Acknowledgments** Financial support from European Commission (ICT: e-LIFT, Grant Agreement No. 247868) is gratefully acknowledged.

## References

- Arnold C, Serra P, Piqué A (2007) Laser direct-write techniques for printing of complex materials. *MRS Bull* 32:23–31
- Blake JR, Gibson DC (1981) Growth and collapse of a vapour cavity near a free surface. *J Fluid Mech* 111:123–140
- Boutopoulos C, Touloupakis E, Pezzotti I et al (2011) Direct laser immobilization of photosynthetic material on screen printed electrodes for amperometric biosensor. *Appl Phys Lett* 98:093703
- Boutopoulos C, Alloncle AP, Zergioti I, Delaporte P (2013a) A time-resolved shadowgraphic study of laser transfer of silver nanoparticle ink. *Appl Surf Sci* 278:71–76
- Boutopoulos C, Papageorgiou DP, Zergioti I, Papanthanasou AG (2013b) Sticking of droplets on slippery superhydrophobic surfaces by laser induced forward transfer. *Appl Phys Lett* 103:024104
- Brown MS, Kattamis NT, Arnold CB (2011) Time-resolved dynamics of laser-induced micro-jets from thin liquid films. *Microfluid Nanofluidics* 11:199–207
- Brown MS, Brasz CF, Ventikos Y, Arnold CB (2012) Impulsively actuated jets from thin liquid films for high-resolution printing applications. *J Fluid Mech* 709:341–370
- Brujan E-A (2011) Numerical investigation on the dynamics of cavitation nanobubbles. *Microfluid Nanofluidics* 11:511–517
- Chatzipetrou M, Tsekenis G, Tsouti V et al (2013) Biosensors by means of the laser induced forward transfer technique. *Appl Surf Sci* 278:250–254
- Cummins G, Desmulliez MPY (2012) Inkjet printing of conductive materials: a review. *Circuit World* 38:193–213
- Duocastella M, Fernández-Pradas JM, Morenza JL, Serra P (2009) Time-resolved imaging of the laser forward transfer of liquids. *J Appl Phys* 106:084907
- Duocastella M, Fernández-Pradas JM, Serra JLMP (2010) Sessile droplet formation in the laser-induced forward transfer of liquids: a time-resolved imaging study. *Thin Solid Films* 518:5321–5325
- Duocastella M, Kim H, Serra P, Piqué A (2012) Optimization of laser printing of nanoparticle suspensions for microelectronic applications. *Appl Phys A* 106:471–478
- Eggers J (1997) Nonlinear dynamics and breakup of free-surface flows. *Rev Mod Phys* 69:865–929
- Fardel R, Nagel M, Nüesch F et al (2009) Shadowgraphy investigation of laser-induced forward transfer: front side and back side ablation of the triazene polymer sacrificial layer. *Appl Surf Sci* 255:5430–5434
- Kim H, Auyeung RCY, Lee SH et al (2009) Laser forward transfer of silver electrodes for organic thin-film transistors. *Appl Phys A* 96:441–445
- Lapotko D (2009) Optical excitation and detection of vapor bubbles around plasmonic nanoparticles. *Opt Express* 17:2538–2556
- Lewis BR, Kinzel EC, Laurendeau NM et al (2006) Planar laser imaging and modeling of matrix-assisted pulsed-laser evaporation direct write in the bubble regime. *J Appl Phys* 100:033107
- Lynch D, Olson C, Weaver J (1975) Optical properties of Ti, Zr, and Hf from 0.15 to 30 eV. *Phys Rev B* 11:3617–3624
- Nedyalkov NN, Imamova S, Atanasov PA et al (2010) Interaction between ultrashort laser pulses and gold nanoparticles: nanoheater and nanolens effect. *J Nanopart Res* 13:2181–2193
- Palla-Papavlu A, Paraico I, Shaw-Stewart J et al (2010) Liposome micropatterning based on laser-induced forward transfer. *Appl Phys A* 102:651–659
- Rapp L, Ailuno J, Alloncle AP, Delaporte P (2011) Pulsed-laser printing of silver nanoparticles ink: control of morphological properties. *Opt Express* 19:21563–21574
- Robinson PB, Blake JR, Kodama T et al (2001) Interaction of cavitation bubbles with a free surface. *J Appl Phys* 89:8225
- Schiele NR, Corr DT, Huang Y et al (2010) Laser-based direct-write techniques for cell printing. *Biofabrication* 2:032001
- Tsouti V, Boutopoulos C, Goustouridis D et al (2010) A chemical sensor microarray realized by laser printing of polymers. *Sens Actuators B Chem* 150:148–153
- Unger C, Gruene M, Koch L et al (2010) Time-resolved imaging of hydrogel printing via laser-induced forward transfer. *Appl Phys A* 103:271–277
- Wang J, Auyeung RCY, Kim H et al (2010) Three-dimensional printing of interconnects by laser direct-write of silver nanopastes. *Adv Mater* 22:4462–4466
- Yan J, Huang Y, Xu C, Chrisey DB (2012) Effects of fluid properties and laser fluence on jet formation during laser direct writing of glycerol solution. *J Appl Phys* 112:083105